Resolution of the time-harmonic Maxwell equations using discontinuous Galerkin methods and domain decomposition algorithms

Victorita Dolean, Hugo Fol, Stephane Lanteri, Ronan Perrussel

Resolution of the time-harmonic Maxwell equations using discontinuous Galerkin methods and domain decomposition algorithms

V. Dolean [a,b,*], H. Fol [b], S. Lanteri [b], R. Perrussel [b]

[a] *Université de Nice Sophia-Antipolis, Laboratoire J.-A. Dieudonné, Parc Valrose, 06902 Nice Cedex 02*

[b] *INRIA Sophia-Antipolis, 2004 rte des Lucioles, 06902 Sophia-Antipolis Cedex*

Abstract

We present numerical results relative to the resolution of the time-harmonic Maxwell equations discretized by discontinuous Galerkin methods. First, a numerical study of the convergence of discontinuous Galerkin methods which compares different strategies proposed in the literature for the elliptic Maxwell equations, is performed in the two-dimensional case. We also introduce a Schwarz-type domain decomposition algorithm for solving the resulting linear systems; this strategy is evaluated in the three-dimensional case.

Key words: time-harmonic Maxwell's equation, discontinuous Galerkin methods, domain decomposition methods.

1 Introduction

This work is concerned with the numerical resolution of the time-harmonic Maxwell equations discretized by discontinuous Galerkin methods on unstructured tetrahedral meshes. Our motivation for using a discontinuous Galerkin method is the enhanced flexibility compared to the conforming edge element

* Corresponding author.

Email addresses: dolean@math.unice.fr (V. Dolean), Hugo.Fol@inria.fr (H. Fol), Stephane.Lanteri@inria.fr (S. Lanteri), Ronan.Perrussel@inria.fr (R. Perrussel).

method [12]: for instance, dealing with non-conforming meshes is straightforward and the choice of the local approximation space is not constrained. Nonetheless, before taking full advantage of these features, it is required to carefully study the basic ingredients of the method such as the choice of the numerical flux at the interface between neighboring elements. In the context of time-harmonic problems, the design of efficient solution strategies for the resulting sparse linear systems is an equally important question.

Previous works have shown convergence results for discontinuous Galerkin methods applied to the time-harmonic Maxwell equations, studied under the form of second-order vector wave equations. Most of these works use a mixed formulation [13,11] but discontinuous Galerkin methods on the non-mixed formulation have recently been proved to converge (interior penalty technique [10,2] and local discontinuous Galerkin method [2]). However, to our knowledge, no direct convergence analysis on the first-order time-harmonic system (1) has been conducted so far, which should be useful, for instance, when using an upwind flux (see subsection 2.3). A first contribution of this work is a numerical study of the convergence of discontinuous Galerkin methods based on centered and upwind fluxes applied to the first-order time-harmonic Maxwell in the two-dimensional case. These methods have previously been shown to be convergent in the time-domain case [9,8]. In a second part, we deal with the resolution of the linear system resulting from a discontinuous Galerkin method based on a centered flux for the discretization of the three-dimensional first-order time-harmonic Maxwell equations. We consider using in this context, a Schwarz-type domain decomposition algorithm based on a first-order condition at interfaces between neighboring subdomains. This condition corresponds to a Dirichlet condition for characteristic variables associated to incoming waves [5].

2 Discretization of the first-order time-harmonic Maxwell system

2.1 Continuous problem

The system of non-dimensionalized time-harmonic Maxwell's equations can be written under the following form:

$$\begin{cases} \mathrm{i}\omega\varepsilon_r \boldsymbol{E} - \mathrm{curl}\ \boldsymbol{H} = -\boldsymbol{J}, \\ \mathrm{i}\omega\mu_r \boldsymbol{H} + \mathrm{curl}\ \boldsymbol{E} = 0, \end{cases} \tag{1}$$

where $\boldsymbol{E}$ and $\boldsymbol{H}$ are the unknown electric and magnetic fields and $\boldsymbol{J}$ is a known current source. The parameters ε_r and μ_r are respectively the complex-valued

relative dielectric permittivity (integrating the electric conductivity) and the relative magnetic permeability; we consider here the case of linear isotropic media. The angular frequency of the problem is given by ω. We solve Equations (1) in a bounded domain Ω, and on its boundary $\partial\Omega = \Gamma_a \cup \Gamma_m$, we impose the following boundary conditions:

$$\begin{aligned} &\text{- a perfect electric conductor condition on } \Gamma_m, \ \textit{ie}\text{: } \boldsymbol{n} \times \boldsymbol{E} = 0 \text{ on } \Gamma_m, \\ &\text{- a Silver-Müller (first-order absorbing boundary) condition on } \Gamma^a, \ \textit{ie}\text{: } \\ &\boldsymbol{n} \times \boldsymbol{E} - \boldsymbol{n} \times (\boldsymbol{H} \times \boldsymbol{n}) = (\boldsymbol{n} \times \boldsymbol{E}^{\text{inc}} - \boldsymbol{n} \times (\boldsymbol{H}^{\text{inc}} \times \boldsymbol{n})) \text{ on } \Gamma_a. \end{aligned} \tag{2}$$

The vectors $\boldsymbol{E}^{\text{inc}}$ and $\boldsymbol{H}^{\text{inc}}$ represent the components of an incident electromagnetic wave. We can further rewrite (1)+(2), assuming $\boldsymbol{J}$ equals to 0, under the following form:

$$\begin{cases} \mathrm{i}\omega G_0 \boldsymbol{W} + G_x \partial_x \boldsymbol{W} + G_y \partial_y \boldsymbol{W} + G_z \partial_z \boldsymbol{W} = 0 \text{ in } \Omega, \\ (M_{\Gamma_m} - G_{\boldsymbol{n}})\boldsymbol{W} = 0 \text{ on } \Gamma_m, \\ (M_{\Gamma_a} - G_{\boldsymbol{n}})(\boldsymbol{W} - \boldsymbol{W}_{\text{inc}}) = 0 \text{ on } \Gamma_a. \end{cases} \tag{3}$$

where $\boldsymbol{W} = (\boldsymbol{E}, \boldsymbol{H})^t$ is the new unknown vector and $G_0 = \begin{pmatrix} \varepsilon_r I_3 & 0_{3\times 3} \\ 0_{3\times 3} & \mu_r I_3 \end{pmatrix}$.

Denoting by $(\boldsymbol{e}^x, \boldsymbol{e}^y, \boldsymbol{e}^z)$ the canonical basis of $\mathbb{R}^3$, the matrices G_l with $l \in \{x, y, z\}$ are given by:

$$G_l = \begin{pmatrix} 0_{3\times 3} & N_{\boldsymbol{e}^l} \\ N^t_{\boldsymbol{e}^l} & 0_{3\times 3} \end{pmatrix} \text{ where for a vector } \boldsymbol{n}, \ N_{\boldsymbol{n}} = \begin{pmatrix} 0 & \boldsymbol{n}_z & -\boldsymbol{n}_y \\ -\boldsymbol{n}_z & 0 & \boldsymbol{n}_x \\ \boldsymbol{n}_y & -\boldsymbol{n}_x & 0 \end{pmatrix}.$$

In the following we denote by $G_{\boldsymbol{n}}$ the sum $G_x \boldsymbol{n}_x + G_y \boldsymbol{n}_y + G_z \boldsymbol{n}_z$ and by $G^+_{\boldsymbol{n}}$ and $G^-_{\boldsymbol{n}}$ its positive and negative parts [1]. We also define $|G_{\boldsymbol{n}}| = G^+_{\boldsymbol{n}} - G^-_{\boldsymbol{n}}$. In order to take into account the boundary conditions, the matrices M_{Γ_m} and M_{Γ_a} are given by:

[1] If $G_{\boldsymbol{n}} = T\Lambda T^{-1}$ is the eigenfactorization then $G^{\pm}_{\boldsymbol{n}} = T\Lambda^{\pm}T^{-1}$ where Λ^+ (resp. Λ^-) only gathers the positive (resp. negative) eigenvalues.

$$M_{\Gamma_m} = \begin{pmatrix} 0_{3\times 3} & N_{\boldsymbol{n}} \\ -N_{\boldsymbol{n}}^t & 0_{3\times 3} \end{pmatrix} \text{ and } M_{\Gamma_a} = |G_{\boldsymbol{n}}|.$$

See [4] for further details on the derivation of this formulation.

2.2 Discretization

Let Ω_h denote a discretization of the domain Ω into a union of conforming elements (tetrahedral or hexahedral elements) $\overline{\Omega}_h = \bigcup_{K\in\mathcal{T}_h} K$. We look for the approximate solutions $(\boldsymbol{E}_h, \boldsymbol{H}_h)^t$ of (3) in $V_h \times V_h$ where the function space V_h is defined by:

$$V_h = \left\{ \boldsymbol{V} \in [L^2(\Omega)]^3 \ / \ \forall K \in \mathcal{T}_h, \quad \boldsymbol{V}_{|K} \in \mathcal{P}(K) \right\}. \tag{4}$$

where $\mathcal{P}(K)$ denotes a space of polynomial functions on the element K. We take the scalar product of the first equation of (3) by a sufficiently smooth vector field $\boldsymbol{V}$ and we integrate over an element K of the mesh $\mathcal{T}_h$:

$$\int_K \mathrm{i}\omega G_0 \boldsymbol{W} \cdot \overline{\boldsymbol{V}} dx + \int_K \sum_{l\in\{x,y,z\}} G_l \partial_l \boldsymbol{W} \cdot \overline{\boldsymbol{V}} dx = 0.$$

By using Green's formula we obtain a weak formulation involving a boundary term $\Phi_{\partial K}$ that requires a specific treatment and which is usually referred as a numerical flux (see also Ern and Guermond [6,7]):

$$\int_K \mathrm{i}\omega G_0 \boldsymbol{W} \cdot \overline{\boldsymbol{V}} dx - \int_K \boldsymbol{W} \cdot \sum_{l\in\{x,y,z\}} G_l \partial_l \overline{\boldsymbol{V}} dx + \int_{\partial K} \Phi_{\partial K}(\boldsymbol{W}) \cdot \overline{\boldsymbol{V}} = 0. \tag{5}$$

In order to couple the element K with its neighbors for ensuring the consistency of the discretization, this numerical flux can be defined in the following

way:

$$\Phi_{\partial K} = \begin{cases} I_{FK} S_F [\![\boldsymbol{W}]\!] + I_{FK} G_{\boldsymbol{n}_F} \{\boldsymbol{W}\} \text{ if } F \in \Gamma^0, \\ \dfrac{1}{2}(M_{F,K} + I_{FK} G_{\boldsymbol{n}_F}) \boldsymbol{W} \text{ if } F \in \Gamma^m, \\ \dfrac{1}{2}(M_{F,K} + I_{FK} G_{\boldsymbol{n}_F}) \boldsymbol{W} - \dfrac{1}{2}(M_{F,K} - I_{FK} G_{\boldsymbol{n}_F}) \boldsymbol{W}^{\text{inc}} \text{ if } F \in \Gamma^a, \end{cases} \tag{6}$$

where Γ^0, Γ^a and Γ^m respectively denote the set of interior faces, the set of faces on Γ_a and the set of faces on Γ_m. I_{FK} stands for the incidence matrix between oriented faces and elements whose entries are given by:

$$I_{FK} = \begin{cases} \ \ 0 \text{ if the face } F \text{ does not belong to element } K, \\ \ \ 1 \text{ if } F \in K \text{ and their orientations match}, \\ -1 \text{ if } F \in K \text{ and their orientations do not match}. \end{cases}$$

We also define respectively the jump and the average of $\boldsymbol{W}$ on a face F shared by two elements K and $\tilde{K}$:

$$[\![\boldsymbol{W}]\!] = I_{FK} \boldsymbol{W}_K + I_{F\tilde{K}} \boldsymbol{W}_{\tilde{K}} \text{ and } \{\boldsymbol{W}\} = \frac{1}{2}(\boldsymbol{W}_K + \boldsymbol{W}_{\tilde{K}}).$$

Finally, the matrix S_F allows to penalize the jump of a field or of some components of this given field on the face F and the matrix $M_{F,K}$ to be defined later insures the asymptotic consistency with the boundary conditions of the continuous problem.

2.3 Choice of the numerical flux

In this study, we aim at comparing the properties of three classical numerical fluxes:

- **a centered flux** (see [8] for the time-domain equivalent). In this case $S_F = 0$ for all the faces F and, for the boundary faces, we use:

$$M_{F,K} = \begin{cases} I_{FK} \begin{pmatrix} 0_{3\times 3} & N_{\boldsymbol{n}_F} \\ -N^t_{\boldsymbol{n}_F} & 0_{3\times 3} \end{pmatrix} \text{ if } F \in \Gamma^m, \\ |G_{\boldsymbol{n}_F}| \text{ if } F \in \Gamma^a. \end{cases}$$

- **an upwind flux** (see [6,14]). In this case:

$$S_F = \begin{pmatrix} \alpha_F^E N_{\boldsymbol{n}} N_{\boldsymbol{n}}^t & 0_{3\times 3} \\ 0_{3\times 3} & \alpha_F^H N_{\boldsymbol{n}}^t N_{\boldsymbol{n}} \end{pmatrix}, \; M_{F,K} = \begin{pmatrix} \eta_F N_{\boldsymbol{n}_F} N_{\boldsymbol{n}_F}^t & I_{FK} N_{\boldsymbol{n}_F} \\ -I_{FK} N_{\boldsymbol{n}_F}^t & 0_{3\times 3} \end{pmatrix} \; \forall F \in \Gamma^m,$$

with α_F^E, α_F^H and η_F equals to $1/2$ for homogeneous media. The definition of M_{FK} for F in Γ^a is identical to the centered case.

- **a partially penalized upwind flux** (local Discontinuous Galerkin method, see [3]). This flux is characterized by a penalization coefficient given by:

$$S_F = \tau_F h_F^{-1} \begin{pmatrix} N_{\boldsymbol{n}_F} N_{\boldsymbol{n}_F}^t & 0 \\ 0 & 0 \end{pmatrix}, \; M_{F,K} = \begin{pmatrix} \eta_F h_F^{-1} N_{\boldsymbol{n}_F} N_{\boldsymbol{n}_F}^t & I_{FK} N_{\boldsymbol{n}_F} \\ -I_{FK} N_{\boldsymbol{n}_F}^t & 0_{3\times 3} \end{pmatrix} \; \forall F \in \Gamma^m.$$

The definition of M_{FK} for F in Γ^a is also identical to the centered case.

We are interested in assessing these numerical fluxes for the discretization of (3). Firstly, we want the best asymptotic convergence order in L^2-norm for the electric and magnetic field for a fixed polynomial order approximation on an unstructured mesh. Secondly, a minimal numerical dispersion is also needed. In the following we will focus on the first criterion. The asymptotic convergence order in L^2-norm between the exact solution $(\boldsymbol{E}, \boldsymbol{H})$ and the approximate solution $(\boldsymbol{E}_h, \boldsymbol{H}_h)$ corresponds to the largest real coefficients β and γ such that :

$$\exists C_1, C_2, h_0 > 0, \; \forall h > h_0, \; \|\boldsymbol{E} - \boldsymbol{E}_h\|_{L^2(\Omega)} \leq C_1 h^\beta \text{ and } \|\boldsymbol{H} - \boldsymbol{H}_h\|_{L^2(\Omega)} \leq C_2 h^\gamma,$$

where h is the mesh size.

We first recall in Table 1 below the theoretical convergence order for the elliptic Maxwell equations [6,7], for a sufficiently smooth solution and when the local function space $\mathcal{P}(K)$ is $[P_k(K)]^3$ *i.e.* the space of vectors whose components are polynomials of order at most k. When using flux with a penalization of $\boldsymbol{E}$, similar convergence results are proved for the time-harmonic Maxwell equations in [2].

flux	centered	upwind	penalization of $\boldsymbol{E}$
field $\boldsymbol{E}$	k	$k+1/2$	$k+1$
field $\boldsymbol{H}$	k	$k+1/2$	k

Table 1
Theoretical convergence order for the elliptic Maxwell equations.

2.4 Two-dimensional numerical results

We consider the case of an electric transverse wave in the plane (O, x, y). In this case the components $\boldsymbol{E}_z$, $\boldsymbol{H}_x$ and $\boldsymbol{H}_y$ are zero. We numerically simulate the propagation of a plane wave in vacuum where the incident wave is given by $(\boldsymbol{E}_x^{\text{inc}}, \boldsymbol{E}_y^{\text{inc}}, \boldsymbol{H}_z^{\text{inc}}) = \exp(-i\omega x)(0, 1, 1)$. The computational domain is the unit square $\Omega =]0;1[^2$ and a Silver-Müller boundary condition is imposed on the whole boundary, that is $\Gamma_a = \partial\Omega$ and $\Gamma_m = \emptyset$. The parameters ε_r and μ_r are set to 1 everywhere and we choose $\omega = 2\pi$. We numerically estimate the asymptotic convergence order of discontinuous Galerkin methods for the above problem using two different sequences of triangular meshes:

- **uniformly refined meshes.** The first mesh of Figure 1(a) is uniformly refined resulting in the meshes of Figures 1(b) and 1(c).

- **independent meshes.** We use four unstructured (quasi-uniform) independent meshes with an imposed maximal mesh size h (see Figure 2 for the first three meshes). These meshes are denoted by $\mathcal{T}_i$ for $i = 1, \ldots, 4$ with h in a decreasing order. Thus $\mathcal{T}_{i+1}$ is not a refinement of $\mathcal{T}_i$.

Our implementation of high order discontinuous Galerkin methods makes use of nodal basis functions with equi-spaced nodes.

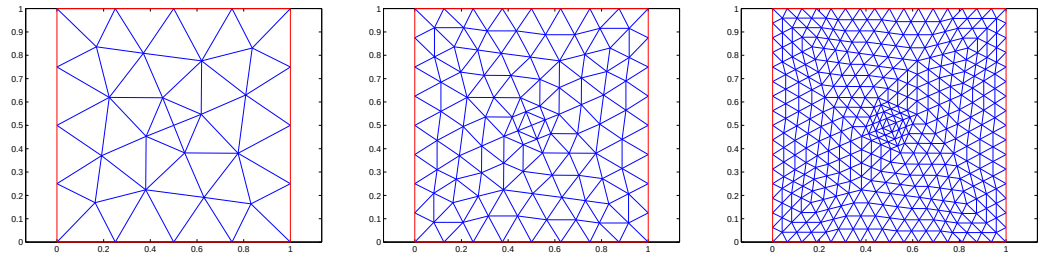

(a) Initial mesh. (b) First refinement. (c) Second refinement.

Fig. 1. Initial mesh of the unit square and two uniform refinements.

2.4.1 Convergence behavior using meshes obtained by uniform refinement

Centered flux. Numerical convergence results in a logarithmic scale are shown on Figure 3. They clearly demonstrate the interest of higher order polynomial approximations which allow a considerable reduction of the number of

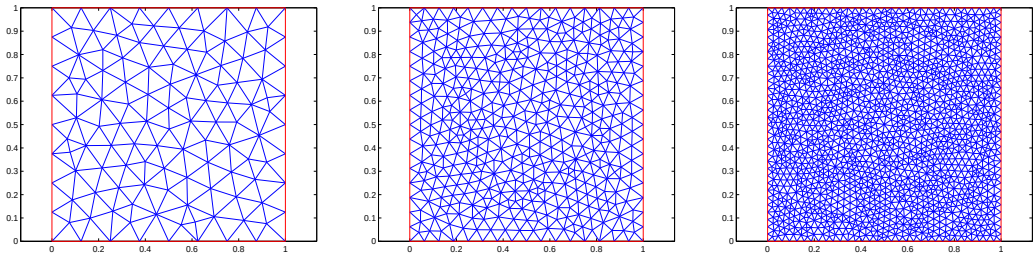

(a) $h = 1/8$. (b) $h = 1/16$. (c) $h = 1/32$.

Fig. 2. First three independent unstructured meshes.

degrees of freedom to reach the same accuracy. Table 2 summarizes numerical estimates (using a linear regression method) of the asymptotic convergence order.

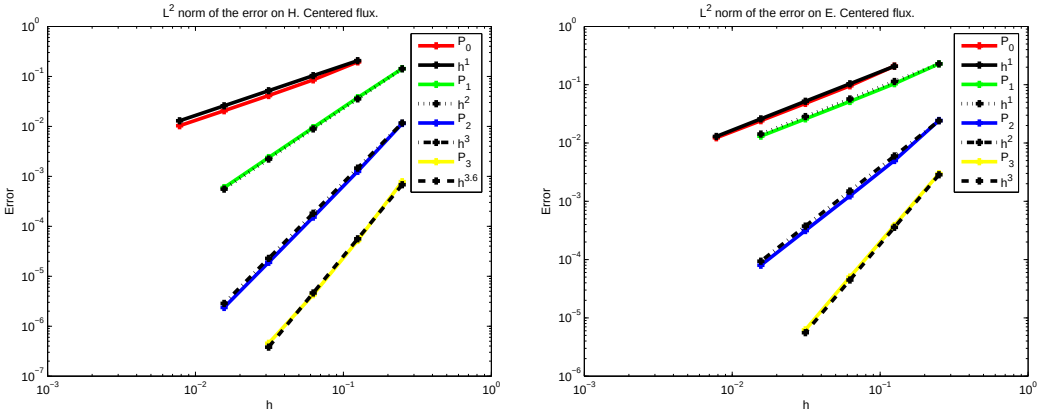

(a) $\|\boldsymbol{H} - \boldsymbol{H}_h\|_{L^2}$ against h. (b) $\|\boldsymbol{E} - \boldsymbol{E}_h\|_{L^2}$ against h.

Fig. 3. Convergence results using a centered flux.

	P_0	P_1	P_2	P_3
$\boldsymbol{E}$	1.02	1.03	2.05	2.97
$\boldsymbol{H}$	1.05	1.98	3.05	3.58

Table 2
Numerical convergence order using a centered flux.

The method based on a P_0 approximation (*i.e.* the standard cell centered finite volume method) is special: the convergence order is optimal for both fields $\boldsymbol{E}$ and $\boldsymbol{H}$, that is, equal to $k+1$. This could be the consequence of using uniformly refined meshes, since a somewhat different behavior is obtained for independent meshes with decreasing mesh size (see subsection 2.4.2). For the other polynomial degrees, we get exactly the predicted theoretical convergence order in the elliptic case for $\boldsymbol{E}$, whereas for $\boldsymbol{H}$, this convergence order is optimal. Therefore, in this example, the magnetic field is better approximated than the electric field, when using the centered flux.

Upwind flux. We used here the parameters $\alpha_F^H = \alpha_F^E = \eta_F = 1$ for each face F. Numerical convergence results are shown on Figure 4. Similar conclusions

can be derived as in the centered case except that the convergence properties of the methods based on P_0 and P_1 interpolations are this time clearly different with respect to the centered case. The asymptotic convergence orders (see Table 3) are similar for both fields and correspond to the theory for the elliptic Maxwell equations. The convergence is optimal except for the case P_0, but nevertheless we are still above the theoretical estimates.

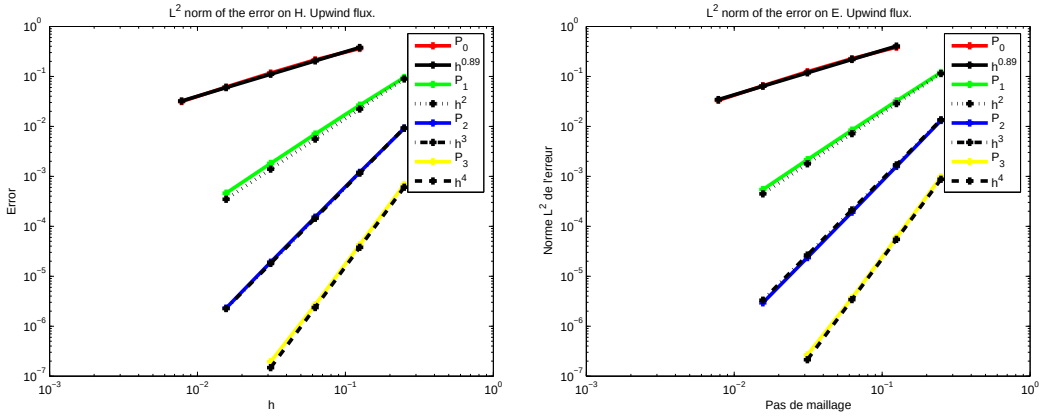

(a) $\|\boldsymbol{H} - \boldsymbol{H}_h\|_{L^2}$ against h. (b) $\|\boldsymbol{E} - \boldsymbol{E}_h\|_{L^2}$ against h.

Fig. 4. Convergence results using an upwind flux.

	P_0	P_1	P_2	P_3
$\boldsymbol{E}$	0.89	1.95	3.03	3.95
$\boldsymbol{H}$	0.89	1.93	2.99	3.93

Table 3
Numerical convergence order using an upwind flux.

Penalized flux on $\boldsymbol{E}$. We set $\tau_F = \eta_F = 1$ for each face F. Results are shown on Figure 5. Table 4 summarizes the numerical estimates of the asymptotic convergence order. Besides the expected lack of convergence in the case P_0, we can notice for all the other cases ($(P_k)_{k>0}$) a complementary behavior with respect to the centered flux, since this time we get an optimal convergence rate for $\boldsymbol{E}$, but not for $\boldsymbol{H}$.

	P_0	P_1	P_2	P_3
$\boldsymbol{E}$	X	1.97	3.05	3.93
$\boldsymbol{H}$	X	0.97	2.02	2.89

Table 4
Numerical convergence order using a penalized flux on $\boldsymbol{E}$.

2.4.2 Convergence behavior using independent meshes

On Figure 6, we compare the evolution of the L^2-norm of the error with the mesh size h by using the meshes $(\mathcal{T}_i)_{i=1,\dots,4}$, for both a centered flux and an upwind flux, Figure 6(b) corresponds to the error for the field $\boldsymbol{E}$ while

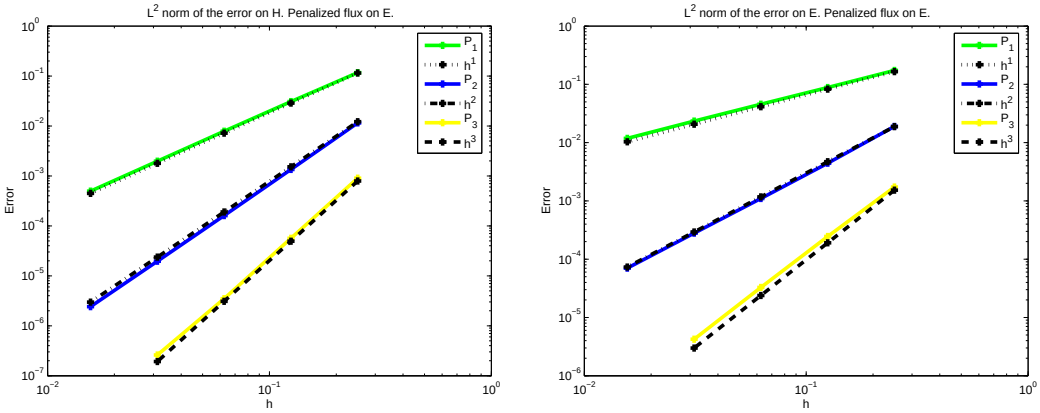

(a) $\|\boldsymbol{H} - \boldsymbol{H}_h\|_{L^2}$ against h. (b) $\|\boldsymbol{E} - \boldsymbol{E}_h\|_{L^2}$ against h.

Fig. 5. Convergence results using a penalized flux on $\boldsymbol{E}$.

Figure 6(a) corresponds to the error for the field $\boldsymbol{H}$. The results for the upwind flux are the same as for the uniformly refined meshes. For the centered flux, note the lack of convergence for the case P_0. For all the other cases the results remain the same as for the uniformly refined meshes.

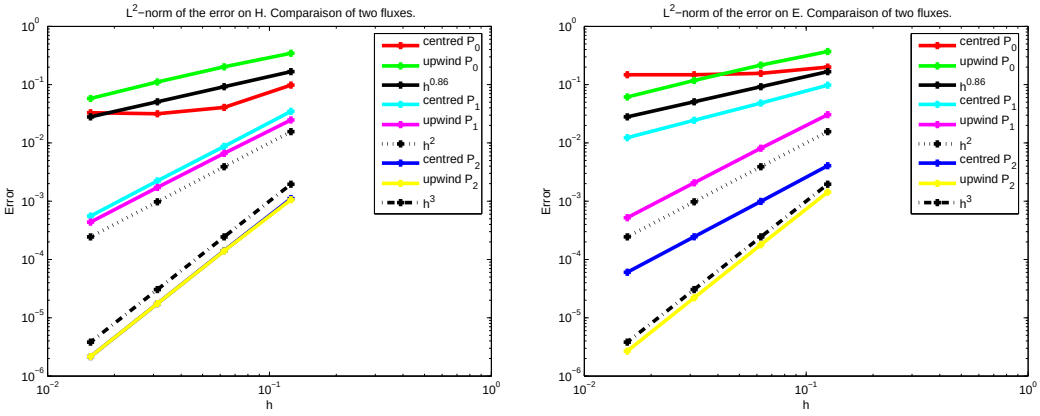

(a) $\|\boldsymbol{H} - \boldsymbol{H}_h\|_{L^2}$ against h. (b) $\|\boldsymbol{E} - \boldsymbol{E}_h\|_{L^2}$ against h.

Fig. 6. Comparison of the convergence results between centered flux and upwind flux.

It is already known for time-domain problems that the centered flux combined to a leap-frog time integration scheme results in a non-dissipative discontinuous Galerkin method (a mandatory feature for long time computations, see [8]). As far as time-harmonic problems are concerned, the previous results show that the upwind flux has better convergence properties. Nevertheless, the centered flux remains less expensive both for time-domain and time-harmonic problems (arithmetic operations and memory requirements). In the following we will show some preliminary numerical results for the three-dimensional problem discretized by a discontinuous Galerkin method based on a centered flux combined to a P_0 or P_1 interpolation in the elements of a tetrahedral mesh.

3 Parallel solvers for the time-harmonic Maxwell system

From now, we assume that the three-dimensional first-order time-harmonic Maxwell system is discretized using a discontinuous Galerkin method based on a centered flux. Inside each element of the mesh (tetrahedra in the present case), the components of the $\boldsymbol{E}$ and $\boldsymbol{H}$ fields are approximated using a P_0 approximation (leading to a standard cell centered finite volume method) or a P_1 approximation.

3.1 Domain decomposition algorithm

The linear systems resulting from the discretization methods adopted here are large and sparse and their condition number grows with the decrease of the mesh size or the increase of the polynomial order. Therefore, if one wants to reach a prescribed accuracy at a manageable computational cost, it is required to look for (almost) scalable resolution strategies. A standard approach for solving these systems calls for sparse direct solvers. However, such an approach is not feasible for reasonably large systems due to the memory requirements of direct solvers. Moreover, parallel computing is a mandatory route for the design of solution algorithms capable of solving problems of realistic importance. Several parallel sparse direct solvers have been developed in the recent years such as MUMPS [1]. Even if these solvers efficiently exploit distributed memory parallel computing platforms and allow to treat very large problems, there is still room for improvements of the situation. In this context, domain decomposition algorithms are popular strategies that can be used to design parallel preconditioning techniques for Krylov type iterative methods or as coordination methods for sparse direct solvers applied at the subdomain level.

Our strategy for the design of parallel solvers in conjunction with discontinuous Galerkin methods on simplicial meshes relies on a Schwarz algorithm where a first-order condition is imposed at the interfaces between neighboring subdomains that corresponds to a Dirichlet condition for characteristic variables associated to incoming waves. From the discretization viewpoint, this interface condition gives rise to a boundary integral term in (5) which is treated using a flux splitting scheme similar to the one applied at absorbing boundaries. This approach is actually a first step prior to considering high-order, optimized, interface conditions and we refer to [5] for a more detailed presentation of these algorithms including convergence analysis results. Note that the Schwarz algorithm can be used as a global solver or it can be reformulated as a Richardson iterative method acting on an interface system. In the latter case, the resolution of the interface system can be performed in a more effi-

cient way using a Krylov method. Concerning computer implementation, the adopted parallelization strategy combines an element-wise partitioning using the MeTiS partitioner, combined to a message passing programming model using the MPI standard.

3.2 Performance evaluation on a model test case

The test case considered here is essentially used for a first validation of the proposed domain decomposition algorithms. The computational domain is the unit cube and a Silver-Müller condition is applied on the whole boundary of the cube. The underlying meshes are constructed as a subdivision of a regular cubic meshes (N_x, N_y and N_z denotes the number of discretization along the x, y and z directions) where each cube yields five tetrahedra.

Numerical experiments are conducted on a cluster of 64 AMD Opteron/2 GHz processors with a Gigabit Ethernet interconnection. Each processor is equipped with 1 GB of RAM memory for a total of 64 GB. The solvers that we consider make use of a BiCGstab(l) Krylov method [15] either for solving the interface system associated with the Schwarz algorithm or as a subdomain solver. Note that the BiCGstab(l) method is here preconditioned either by a full factorization using the MUMPS sparse direct solver [1] or by an ILUT(τ,p) incomplete factorization. In both cases, the factorization is performed in 32 bit floating point arithmetic in order to save memory space; this is the reason why the factorization provided by MUMPS is not directly used to solve the linear system. All other operations are performed in double precision arithmetic.

We compare the performances of the following solvers:

- GLOB: an unpreconditioned BiCGstab(6) method.
- GLOBD: one iteration of a BiCGstab(1) method preconditioned by a MUMPS factorization.
- DDM1: a Schwarz algorithm used as a global solver where the subdomain solver relies on a BiCGstab(6)+ILUT(10^{-3},1000) combination.
- DDM2: BiCGstab(6) applied to the interface system where the the subdomain solver relies on a BiCGstab(6)+ILUT(10^{-3},1000) combination.
- DDM3: BiCGstab(6) applied to the interface system where the the subdomain solver relies on BiCGstab(1)+MUMPS combination.

In the tables below, "CPU" denotes the maximum of the CPU times per processor while "Elapsed" stands for the elapsed execution time. For this test case, we only consider a discontinuous Galerkin method based on a P_0 approximation of the $\boldsymbol{E}$ and $\boldsymbol{H}$ fields. Performance results are given in Tables 5 and 6 for two mesh sizes. The GLOBD solver is clearly the most efficient option. The DDM3 solver exhibits nice scalability properties as should be

expected for such moderately parallel calculations. On the other hand, the domain decomposition based solvers present another advantage over a global factorization method which is related to the memory space used for storing the L and U factors. As a matter of fact, the preprocessor memory usage for storing these factors is 407 MB (min)/452 MB (max) while the corresponding figure for the subdomain factors in the DDM3 solver is 164 MB (this figure is the same for each subdomain in the present case). Finally, the elapsed time for building the factors in the GLOBD and DDM3 solvers is 29.0 sec and 7.0 sec respectively.

Solver	# iter	CPU	Elapsed
GLOBD	1	2.0 sec	3.0 sec
GLOB	383	227.0 sec	239.0 sec
DDM1	> 100	1070.0 sec	1074.0 sec
DDM2	5	698.0 sec	702.0 sec
DDM3	5	59.0 sec	63.0 sec

Table 5
Plane wave propagation in vacuum.
N_x=41, N_y=N_z=15, discontinuous Galerkin method with P_0 approximation.
vertices = 9,225 - # tetrahedra = 47,040 - # dof = 282,240, # procs = 4.

Solver	# procs	# iter	CPU	Elapsed
GLOBD	4	1	3.2 sec	5.5 sec
-	16	1	1.6 sec	5.1 sec
DDMINT3	4	6	157.0 sec	159.0 sec
-	16	7	38.0 sec	40.0 sec

Table 6
Plane wave propagation in vacuum.
N_x=81, N_y=N_z=15, discontinuous Galerkin method with P_0 approximation.
vertices = 18,225 - # tetrahedra = 94,080 - # dof = 564,480.

3.3 Scattering of a plane wave by a perfectly conducting sphere

The next test case is the scattering of a plane wave by a perfectly conducting unit sphere. The incident wave is given by $\boldsymbol{E}^{\text{inc}} = (\exp(-i\omega x), 0, 0)^t$ and $\boldsymbol{H}^{\text{inc}} = (0, \exp(-i\omega x), 0)^t$, with $\omega = 4\pi$. The absorbing boundary is set to one wavelength from the surface of the perfectly conducting sphere. Two tetrahedral meshes have been used for this test case depending on the approximation adopted in the discontinuous Galerkin method:

- P_0 approximation, mesh M1: # vertices = 244,834, # tetrahedra = 1,382,400 and # dof = 8,292,000.
- P_1 approximation, mesh M1: # vertices = 70,422, # tetrahedra = 384,000 and # dof = 9,216,000.

The physical solution in terms of the contour lines of the real part of the component E_x are shown on Figure 7. Note that despite the coarsest mesh used for the discontinuous Galerkin method based on P_1 approximation, the resulting solution is very close to the exact solution. Concerning the solvers used for this test cases, it has not been possible to apply the GLOBD solver (*i.e.* global, parallel, factorization as a preconditioner to the BiCGstab(l) method) with neither of the discontinuous Galerkin methods and tetrahedral meshes considered here, due to the memory space limitation. Moreover, for the same reason, it has not been possible to run the DDM3 solver in combination with the discontinuous Galerkin method based on P_1 approximation. Finally, performance results for the discontinuous Galerkin method based on P_0 approximation are given in Table 7. Note that for the DDM3 solver, the time per processor for performing the factorization is 18.0 sec (min)/102.0 sec (max) while the associated memory usage is 405 MB (min)/1001 MB (max).

Solver	# iter	CPU (min)	CPU (max)	Elapsed
GLOB	2031	1940.0 sec	2142.0 sec	2919.0 sec
DDM3	14	259.0 sec	413.0 sec	449.0 sec

Table 7
Plane wave propagation in vacuum.
Mesh M2, discontinuous Galerkin method with P_0 approximation.
Performance results, # procs = 64.

References

[1] Patrick R. Amestoy, Iain S. Duff, Jean-Yves L'Excellent, and Jacko Koster. A fully asynchronous multifrontal solver using distributed dynamic scheduling. *SIAM J. Matrix Anal. Appl.*, 23(1):15–41 (electronic), 2001.

[2] A. Buffa and I. Perugia. Discontinuous Galerkin approximation of the Maxwell eigenproblem. Technical Report PV-24, IMATI-CNR, 2005.

[3] Bernardo Cockburn and Chi-Wang Shu. The local discontinuous Galerkin method for time-dependent convection-diffusion systems. *SIAM J. Numer. Anal.*, 35(6):2440–2463 (electronic), 1998.

[4] Victorita Dolean, Hugo Fol, Stéphane Lanteri, and Serge Piperno. Méthodes de Galerkin Discontinu pour les équations de Maxwell en régime harmonique. Technical Report 5904, INRIA, September 2005.

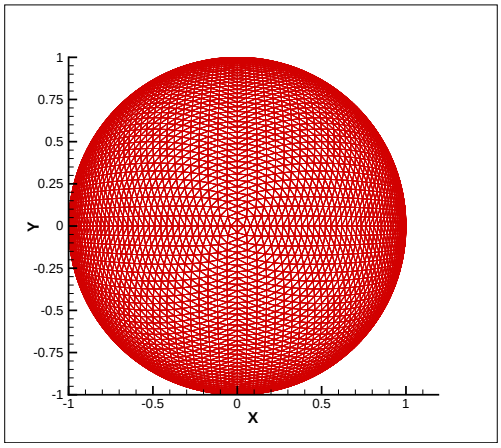

(a) Mesh M1, surfacic mesh.

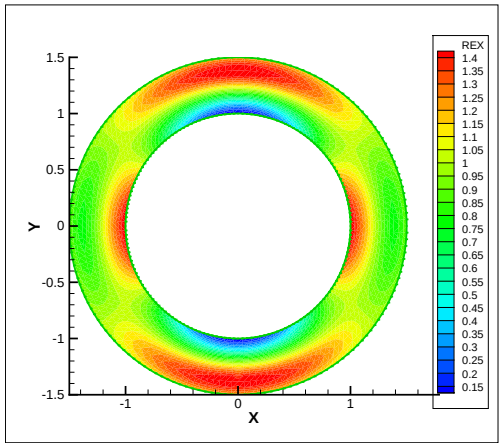

(b) Mesh M1, exact solution.

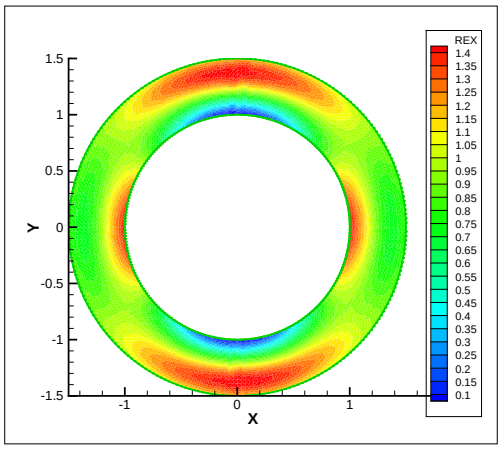

(c) Mesh M2, DG-P0 method.

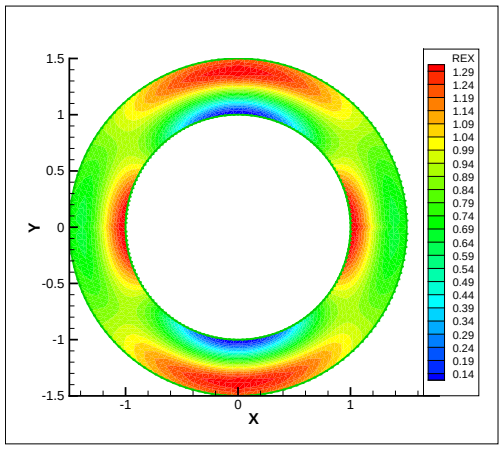

(d) Mesh M1, DG-P1 method.

Fig. 7. Scattering of plane wave by a perfectly conducting sphere.

[5] Victorita Dolean, Martin J. Gander, and Luca Gerardo-Giorda. Why can classical Schwarz methods applied to hyperbolic systems converge even without overlap? In preparation.

[6] Alexandre Ern and Jean-Luc Guermond. Discontinuous Galerkin Methods for Friedrichs' systems. I. General theory. *SIAM J. Numer. Anal.*, 2006. In press.

[7] Alexandre Ern and Jean-Luc Guermond. Discontinuous Galerkin Methods for Friedrichs' systems. II. Second-order elliptic PDE's. *SIAM J. Numer. Anal.*, 2006. In press.

[8] Loula Fezoui, Stéphane Lanteri, Stéphanie Lohrengel, and Serge Piperno. Convergence and stability of a discontinuous Galerkin time-domain method for the 3D heterogeneous Maxwell equations on unstructured meshes. *M2AN Math. Model. Numer. Anal.*, 39(6):1149–1176, 2005.

[9] J. S. Hesthaven and T. Warburton. Nodal high-order methods on unstructured grids. I. Time-domain solution of Maxwell's equations. *J. Comput. Phys.*,

181(1):186–221, 2002.

[10] Paul Houston, Ilaria Perugia, Anna Schneebeli, and Dominik Schötzau. Interior penalty method for the indefinite time-harmonic Maxwell equations. *Numer. Math.*, 100(3):485–518, 2005.

[11] Paul Houston, Ilaria Perugia, Anna Schneebeli, and Dominik Schötzau. Mixed discontinuous Galerkin approximation of the Maxwell operator: the indefinite case. *M2AN Math. Model. Numer. Anal.*, 39(4):727–753, 2005.

[12] Peter Monk. *Finite element methods for Maxwell's equations*. Numerical Mathematics and Scientific Computation. Oxford University Press, New York, 2003.

[13] I. Perugia, D. Schötzau, and P. Monk. Stabilized interior penalty methods for the time-harmonic Maxwell equations. *Comput. Methods Appl. Mech. Engrg.*, 191(41-42):4675–4697, 2002.

[14] Serge Piperno. L^2-stability of the upwind first order finite volume scheme for the Maxwell equations in two and three dimensions on arbitrary unstructured meshes. *M2AN Math. Model. Numer. Anal.*, 34(1):139–158, 2000.

[15] Gèrard L. G. Sleijpen and Diederik R. Fokkema. BiCGstab(l) for linear equations involving unsymmetric matrices with complex spectrum. *Electron. Trans. Numer. Anal.*, 1(Sept.):11–32 (electronic only), 1993.